



A numerical examination of the far-field hydrodynamics of a swimmer near a wall

THESIS

submitted in partial fulfillment of the
requirements for the degree of

MASTER OF SCIENCE

in

PHYSICS

Author :	M.H. Teunisse
Student ID :	1858408
Supervisor :	Luca Giomi
2 nd corrector :	Daniela Kraft

Leiden, The Netherlands, December 17, 2020

A numerical examination of the far-field hydrodynamics of a swimmer near a wall

M.H. Teunisse

Huygens-Kamerlingh Onnes Laboratory, Leiden University
P.O. Box 9500, 2300 RA Leiden, The Netherlands

December 17, 2020

Abstract

The hydrodynamic properties of self-propelled particles have, in the past, been approximated by a multipole expansion. As it becomes easier to produce synthetic swimmers in various shapes and sizes, a proper understanding of this hydrodynamic basis will likely be important. In this thesis, simulation was used to explore the diffusive behavior of the first-order term in the presence of a wall. To quantify this behavior, the characteristic rotation time and effective diffusion coefficient were determined for a range of values of the first-order expansion coefficient α . It is shown that for low α the particle diffuses in three dimensions, while for high α it diffuses in two dimensions as it is locked parallel to the wall.

Contents

1	Introduction	7
1.1	Motivation	7
1.2	Overview	8
2	Methods	9
2.1	Nomenclature	9
2.2	Theory	10
2.2.1	Equations of motion for an active particle	11
2.2.2	Hydrodynamic stress on a moving particle	14
2.2.3	Simplification of hydrodynamic stress near a wall	15
2.3	Simulation	18
2.3.1	General properties	18
2.3.2	Simulating the trajectory of an active particle	18
2.3.3	Boundary correction	20
3	Results	23
3.1	Qualitative observations of particle trajectory	23
3.2	Quantification by mean-squared displacement and velocity-velocity correlation	24
3.3	Determination of diffusion coefficient and rotation time	25
3.4	Analytical calculation	27
4	Discussion	29
4.1	Limitations of simulation	29
4.2	Higher-order terms	29
4.3	Application to experiments	30
5	Conclusions	31

Introduction

When one places a particle in a fluid, the resulting motion can be separated into passive and active motion. A passive colloid will be subject to random fluctuations that make it perform a random walk. This phenomenon, called Brownian motion, has been extensively studied. A more recent field of study is that of active particles, which are capable of performing directed motion. This directed motion can be driven by various mechanisms. For self-propelled particles, a subset of active particles, the particles use up energy from their environment on an individual level.

In biological systems, active and particularly self-propelled motion is very common. This type of movement is not exclusive to living objects, though. The study of active particles is relevant both as a way to better understand the active motion seen in biological systems, and to make the construction of artificial active systems possible.

1.1 Motivation

Research into active particles started with living cells, such as bacteria[1] and sperm cells[2]. More recently, synthetic swimmers such as bimetallic Janus rods[3], artificial flagella[4] and catalytically propelled Pt-coated swimmers[5] were realized.

Due to advancements in 3D-printing, it is now possible to print particles with a sub-micrometer resolution. The production of catalytically propelled active particles by 3D printing was recently investigated[6]. This method makes it possible to create self-propelled particles with a wide variety of shapes. It will therefore be useful to establish a strong basis for

the behavior of active particles of different shapes and sizes. Simulation is an attractive way to approach this problem, as the relevant effects can be incorporated one at a time.

1.2 Overview

The aim of this thesis is to review the existing hydrodynamic theory of active particles, and to make it more easily applicable to experiments. In particular, we focus on the hydrodynamic interactions between a swimmer and a nearby no-slip wall. Using multipole expansion[7], we demonstrate that swimmers crossover from three- to two-dimensional diffusion.

Chapter 2

Methods

2.1 Nomenclature

μ = (dynamic) viscosity of the surrounding fluid

\vec{x}_0 = particle position

\vec{x} = position of a point in the fluid

v_0 = active velocity in infinite fluid

\vec{p} = direction of active velocity

\vec{v} = total particle velocity

\vec{u} = velocity field of surrounding fluid

p = pressure field of surrounding fluid

a = radius of sphere/semimajor axis length of ellipsoidal particle

b = semiminor axis length of ellipsoidal particle

$e = \frac{b}{a}$ = eccentricity of ellipsoidal particle

$\Gamma = \frac{1-e}{1+e}$

θ = out-of-plane angle of particle with respect to the x-y plane

ϕ = in-plane angle of the particle with respect to the x axis

ξ = rapidly fluctuating noise

D = diffusion coefficient

τ_r = rotation time

$\alpha, \beta, \gamma, \tau$ = multipole expansion coefficients (see subsection 2.2.2)

2.2 Theory

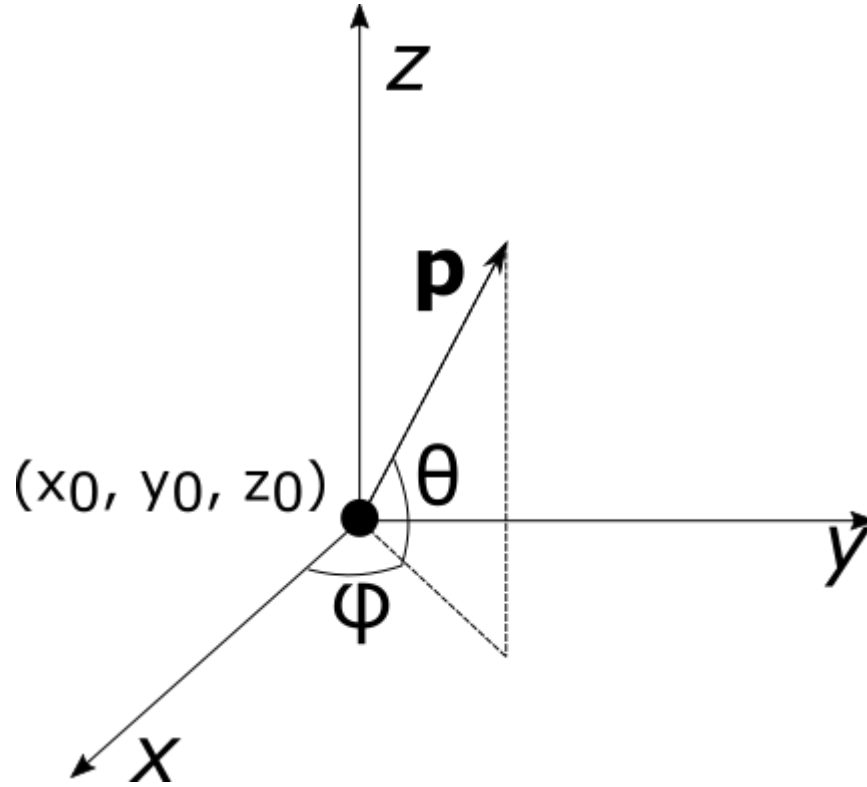


Figure 2.1: Schematic illustration of the relevant coordinates.

This thesis considers the active diffusion of a particle which is axisymmetrical about its direction of motion \vec{p} . Such a particle is characterized by five coordinates. These are the center-of-mass coordinates $\vec{x}_0=(x_0, y_0, z_0)$, and the spherical coordinates θ, ϕ that give the orientation of the vector \vec{p} . The particle is moving near a boundary, represented as an infinite plane at $z = 0$ spanning the x - y -plane. The spherical coordinates are chosen such that ϕ is the angle in the x - y plane and θ is the azimuthal angle. Although the convention for spherical coordinates is to set $\theta = 0$ when the vector lies along the z axis, it is more convenient here to set $\theta = 0$ when \vec{p} lies in the x - y plane. Thus, \vec{p} in Cartesian coordinates takes the form

$$\vec{p} = (\cos \theta \cos \phi, \cos \theta \sin \phi, \sin \theta) \quad (2.1)$$

Subsection 2.2.1 describes the equations of motion for an infinite fluid, first for a passive particle and then for an active particle. Subsection

2.2.2 describes how this motion is influenced by hydrodynamics, both in an infinite fluid and near a wall. Finally, subsection 2.2.3 describes the simplifications that are used to obtain equations of motion for an active particle near a wall.

2.2.1 Equations of motion for an active particle

Fundamentals of Brownian motion

When a particle is suspended in a fluid, it is pushed around by the random motion of the surrounding molecules. These collisions make the larger particle perform a random walk. This is called Brownian motion, and is described in 1D by the equation

$$\frac{dx_k}{dt} = \xi_k(t) \quad (2.2)$$

where $\xi_k(t)$ is rapidly fluctuating noise and x_k is a generic coordinate. In general, it is not necessary to know $\xi_k(t)$ in full. Instead, it is often sufficient to know only its first and second moments. Let it be assumed that there is no drift, that there is no correlation between the noise at different time points and that the statistical properties of the noise do not change overtime. The mean of the noise is then:

$$\langle \xi_k(t) \rangle = 0 \quad (2.3)$$

and its autocorrelation function is a delta function:

$$\langle \xi_k(t_1) \xi_k(t_2) \rangle = 2D_k \delta(t_1 - t_2) \quad (2.4)$$

where D_k is the diffusion coefficient.

For diffusion in multiple dimensions, Equation 2.2 becomes a vector equation:

$$\frac{d\vec{x}_k}{dt} = \vec{\xi}_k(t) \quad (2.5)$$

The mean-squared displacement

Integration of equation 2.2 over time gives the displacement $x_k(t)$ of the particle:

$$x_k(t) = \int_0^t dt' \frac{dx_k(t')}{dt'} = \int_0^t dt' \xi_k(t') \quad (2.6)$$

Because the average displacement of the particle is always $\langle x_k(t) \rangle = 0$ in the absence of drift, the mean-squared displacement $\langle x_k^2(t) \rangle$ is instead used to characterize diffusion. It follows from Equation 2.4 that

$$\langle x_k^2(t) \rangle = 2D_k t \quad (2.7)$$

For a d -dimensional vector \vec{x}_k , the mean-squared displacements of the components are added together:

$$\langle |\vec{x}_k|^2(t) \rangle = \sum_{i=1}^d \langle x_{k,i}(t)^2 \rangle \quad (2.8)$$

so if diffusion is isotropic, the mean-squared displacement in d dimensions is

$$\langle |\vec{x}_k|^2(t) \rangle = 2dDt \quad (2.9)$$

The Langevin equations for an active particle in an infinite fluid

An active particle is a particle that, in addition to Brownian motion, has a velocity $v_0 \vec{p}$. While the velocity v_0 will be assumed constant, the unit vector \vec{p} is subject to rotational diffusion. The simplest case of this is the 2D case, where $\vec{p} = (\cos \theta, \sin \theta)$ and the equations of motion are

$$\begin{aligned} \frac{d\vec{x}_0}{dt} &= v_0 \vec{p}(\theta) + \vec{\xi}_x(t) \\ \frac{d\theta}{dt} &= \xi_\theta(t) \end{aligned} \quad (2.10)$$

Since two angles θ, ϕ describe the orientation of a 3D vector, the full set of equations of motion for an active particle in 3D is

$$\begin{aligned} \frac{d\vec{x}_0}{dt} &= v_0 \vec{p}(\theta, \phi) + \vec{\xi}_x(t) \\ \frac{d\theta}{dt} &= \xi_\theta(\theta, t) \\ \frac{d\phi}{dt} &= \xi_\phi(\theta, t) \end{aligned} \quad (2.11)$$

The equations for the rotational diffusion have a θ dependence here because θ, ϕ are lab frame coordinates rather than body frame coordinates. This is discussed in more detail in Section 2.3.

The combination of an active velocity $v_0 \vec{p}$ with rotational diffusion results

in a trajectory that is ballistic at short timescales and diffusive at long timescales. This is called a persistent random walk. The equations may be simplified by leaving out $\vec{\xi}_x(t)$, as it only adds a random walk on top of this persistent random walk.

Derivation of the mean-squared displacement for an active particle

The mean-squared displacement for a 2D active particle is[8]:

$$\begin{aligned} \langle |\vec{x}_0|^2 \rangle &= 4Dt + v_0^2 \int_0^t dt_1 \int_0^{t_1} dt_2 \langle \vec{p}(t_1) \cdot \vec{p}(t_2) \rangle \\ &= 4Dt + v_0^2 \int_0^t dt_1 \int_0^{t_1} dt_2 \langle \vec{p}(0) \cdot \vec{p}(t_2 - t_1) \rangle \end{aligned} \quad (2.12)$$

Working out the velocity-velocity correlation $\langle \vec{p}(0) \cdot \vec{p}(\Delta t) \rangle$:

$$\begin{aligned} \langle \vec{p}(0) \cdot \vec{p}(\Delta t) \rangle &= \langle \cos \theta(0) \cdot \cos \theta(\Delta t) \rangle + \langle \sin \theta(0) \cdot \sin \theta(\Delta t) \rangle \\ &= \langle \cos \theta(\Delta t) \rangle \\ &= \langle e^{i\theta(\Delta t)} \rangle - i \langle \sin \theta(\Delta t) \rangle = \langle e^{i\theta(\Delta t)} \rangle \end{aligned} \quad (2.13)$$

using that $\theta(0) = 0$.

Since $\theta(\Delta t)$ is an integral of random noise (see Eq. 2.6 with $k = \theta$), it is Gaussian distributed with a variance $2D_\theta t$ (Eq. 2.8). This means that the velocity-velocity correlation becomes a Gaussian integral:

$$\begin{aligned} \langle \vec{p}(0) \cdot \vec{p}(\Delta t) \rangle &= \frac{1}{\sqrt{4\pi D_\theta \Delta t}} \int_{-\infty}^{\infty} d\theta \exp \frac{1}{2} \left(\frac{\theta^2}{2D_\theta \Delta t} + i\theta \right) \\ &= e^{-D_\theta |\Delta t|} \end{aligned} \quad (2.14)$$

Substituting this back into Equation 2.12, one obtains

$$\begin{aligned} \langle |\vec{x}_0|^2 \rangle &= 4Dt + v_0^2 \int_0^t dt_1 \int_0^{t_1} dt_2 e^{-D_\theta |t_2 - t_1|} \\ &= 4Dt + 2v_0^2 \tau_r^2 \left(\frac{t}{\tau_r} + e^{-t/\tau_r} - 1 \right) \end{aligned} \quad (2.15)$$

where τ_r is the rotation time.

In general, the rotation time is defined as the characteristic decay time of the velocity-velocity correlation:

$$\langle \vec{p}(0) \cdot \vec{p}(t) \rangle = e^{-t/\tau_r} \quad (2.16)$$

so in this case, $\tau_r = D_\theta^{-1}$.

The derivation of the 3D mean-squared displacement is very similar. In that case, because there is rotational diffusion in two directions, one obtains for the velocity-velocity correlation:

$$\langle \vec{p}(0) \cdot \vec{p}(\Delta t) \rangle = \langle \cos \theta(\Delta t) \rangle \langle \cos \phi(\Delta t) \rangle = e^{-(D_\theta + D_\phi)\Delta t} \quad (2.17)$$

so the 3D mean-squared displacement is

$$\langle |\vec{x}_0|^2 \rangle = 6Dt + 2v_0^2 \tau_r^2 \left(\frac{t}{\tau_r} + e^{-t/\tau_r} - 1 \right) \quad (2.18)$$

with $\tau_r = (D_\theta + D_\phi)^{-1}$. For an axisymmetrical particle, rotational diffusion is isotropic, so $D_\phi = D_\theta$.

2.2.2 Hydrodynamic stress on a moving particle

Stokes drag in an infinite fluid

The fluid flow at low Reynolds numbers is described by the linearized Navier-Stokes equations:

$$\begin{aligned} \nabla \cdot \vec{u} &= 0 \\ \nabla p &= \mu \nabla^2 \vec{u} \end{aligned} \quad (2.19)$$

where $\vec{u}(\vec{x})$ is the velocity field of the fluid, $p(\vec{x})$ is the pressure field and μ is the viscosity.

From the velocity and pressure fields of the fluid follows the hydrodynamic stress tensor:

$$\sigma_{ij}(\vec{x}) = -p(\vec{x})\delta_{ij} + \mu \left(\frac{\partial u_i(\vec{x})}{\partial x_j} + \frac{\partial u_j(\vec{x})}{\partial x_i} \right) \quad (2.20)$$

Integration of this stress tensor over the particle surface gives the hydrodynamic drag:

$$\vec{F}_d = \oint \! \! \! \oint dS \bar{\sigma} \cdot \vec{n} \quad (2.21)$$

For an axisymmetrical particle moving with some velocity \vec{v} in an infinite fluid, one finds that this force is a drag in the direction opposite the velocity. For a sphere, this drag is described by the well-known Stokes law:

$$\vec{F}_d = -6\mu a \vec{v} \quad (2.22)$$

For an active particle, the active force \vec{F}_a competes with the hydrodynamic drag. The balance between these two forces sets the active velocity v_0 :

$$v_0 = \frac{F_a}{6\mu a} \quad (2.23)$$

When the particle approaches a boundary, the translational symmetry in one direction is broken, causing the hydrodynamic stress to become more complex.

Near a boundary: the method of images

For a particle moving near a solid wall, the fluid needs to obey the boundary conditions at the wall. Let it be assumed that the boundary has the no-slip condition $\vec{u}(z = 0) = 0$. One way to solve this boundary problem is to set a mirror image of the particle at the other side of the boundary. The fields from the particle and those from its mirror image then cancel each other out at the boundary. This is called the method of images. Blake[9] used this method to work out the velocity and pressure fields caused by a point force (called a Stokeslet) in proximity of a boundary.

2.2.3 Simplification of hydrodynamic stress near a wall

To find the force on the particle, one must first determine the velocity field $\vec{u}(\vec{x})$ and pressure field $p(\vec{x})$ that result from its movement. From this one can find the stress tensor $\bar{\sigma}(\vec{x})$. By integrating the product of the fluid stress tensor with the surface normal over the particle surface, one finds the total force (Eq.2.21).

It is very time-consuming to carry out this full calculation for a specific particle shape and propulsion mechanism. In this section, two simplifications will be laid out, namely the multipole expansion of the fluid field and Faxén's laws for the velocity of the particle in a fluid.

Faxén's laws

Faxén's laws provide an approximation of the drag on the particle that is described by Equation 2.21. Provided that $a \ll \nabla^2 \vec{u}(\vec{x}_0)$, the induced

velocity of the particle from the hydrodynamic flow is[7]

$$\begin{aligned}\vec{v}_{ind} &= \vec{u}(\vec{x}_0) + \mathcal{O}(a^2 \nabla^2 \vec{u}(\vec{x}_0)) \\ \Omega_{ind} &= \frac{1}{2} \nabla \times \vec{u}(\vec{x}_0) + \Gamma \vec{p} \times (\vec{p} \cdot (\nabla \vec{u}(\vec{x}_0) + [\nabla \vec{u}(\vec{x}_0)]^T)) / 2 + \mathcal{O}(a^2 \nabla^2 (\nabla \times \vec{u})|_{\vec{x}_0})\end{aligned}\quad (2.24)$$

The multipole expansion of fundamental singularities

Because of the linearity of the Navier-Stokes equations at low Reynolds numbers, solutions can be expressed in terms of singularity solutions. This approach was described in detail by Spagnolie & Lauga (2012)[7]. A brief description is given here.

In an infinite fluid, the disturbance of the velocity field caused by a point force

$$\vec{f}(\vec{x}) = f \vec{p} \delta(\vec{x} - \vec{x}_0) \quad (2.25)$$

takes the form

$$\begin{aligned}\vec{u}(\vec{x}) &= \frac{f}{8\pi\mu|\vec{x} - \vec{x}_0|} \left(\vec{p} + \frac{[\vec{p} \cdot (\vec{x} - \vec{x}_0)](\vec{x} - \vec{x}_0)}{|\vec{x} - \vec{x}_0|^2} \right) \\ &= \frac{f}{8\pi\mu r} \left(\vec{p} + \frac{[\vec{p} \cdot \vec{r}]\vec{r}}{r^2} \right)\end{aligned}\quad (2.26)$$

with $\vec{r} = \vec{x} - \vec{x}_0$. For an extended particle exerting a force $\vec{f}(\vec{x})$ on the fluid, the solution contains an integral over the particle surface[10]:

$$\vec{u}(\vec{x}) = \frac{1}{8\pi\mu} \iint_{\delta S} dS(\vec{y}) \overline{\overline{G}}(\vec{x} - \vec{y}) \cdot \vec{f}(\vec{y}) \quad (2.27)$$

where $\overline{\overline{G}}$ is the Oseen-Green tensor, defined as

$$G_{ij} = \frac{1}{r} \left(1 + \frac{r_i r_j}{r^2} \right) \quad (2.28)$$

so that the dot product of $\overline{\overline{G}}(\vec{x} - \vec{x}_0)$ with $\frac{f}{8\pi\mu} \vec{p}$ gives the velocity field at the point \vec{x} originating from a point force $f \vec{p}$ applied at the point \vec{x}_0 .

With exception for a limited class of highly symmetric surfaces, the integral 2.27 cannot be expressed in terms of elementary functions. Yet, through a Taylor expansion of the Oseen-Green tensor $\overline{\overline{G}}$, one can cast the velocity field \vec{u} as a superposition of elementary flows resulting from increasingly

symmetric distributions of point forces. In analogy with electrodynamics, the latter is referred to as multipole expansion.

In addition, one can always add solutions to the homogeneous equation, which in this case is the Laplace equation $\nabla^2 \vec{u} = 0$. These are referred to as source terms, and are set by the boundary conditions that are imposed by the finite size of the particle.

The solution for the velocity field of an axisymmetric particle can thus be expanded as:

$$\vec{u}(\vec{x}) = \alpha \vec{G}_D(\vec{p}, \vec{p}) + \beta \vec{D}(\vec{p}) + \gamma \vec{G}_Q(\vec{p}, \vec{p}, \vec{p}) + \tau \vec{R}_D(\vec{p}) + \mathcal{O}(|\vec{x} - \vec{x}_0|^{-4}) \quad (2.29)$$

where \vec{G}_D is the force dipole solution, \vec{D} is the source dipole solution, \vec{G}_Q is the force quadrupole solution and \vec{R}_D is the rotlet dipole solution which is present for chiral particles. Full expressions for these fundamental singularity solutions are given in section 2.1 of Spagnolie&Lauga[7]. α, β, γ and τ are coefficients of the multipole expansion, the value of which depends on the particle's geometry and propulsion mechanism.

Induced particle velocity near a wall

The fluid field of axisymmetrical particle in an infinite fluid must obey cylindrical symmetry. This means that such a particle can only experience a hydrodynamic force along its axis of movement, and a torque if the particle is chiral. This symmetry is broken when the particle approaches a wall. Still, because there is translational invariance in the x - y plane, the proximity to the wall does not change the particle motion in an arbitrary way. It can only influence the out-of-plane angle θ or the height z_0 , or induce an additional drag in the x - y -plane. This last effect will not be considered here, as it only influences the translational diffusion in the x - y -plane. The new Langevin equations in this situation are

$$\begin{aligned} \frac{d\vec{x}_0}{dt} &= v_0 \vec{p}(t) + \vec{v}_{ind}(\theta, z, t) \\ \frac{d\theta}{dt} &= \Omega_{ind}(\theta, z, t) + \xi_\theta(\theta, t) \\ \frac{d\phi}{dt} &= \xi_\phi(\theta, t) \end{aligned} \quad (2.30)$$

The fluid field in the proximity of a boundary is found using the method of images. This may be done separately for each term in the multipole

expansion. The approximate induced velocity and angular velocity are then found using Faxén's laws. For the force dipole term, the induced velocity and angular velocity are[7]:

$$\begin{aligned}\vec{v}_{ind} &= a^2 v_0 \frac{3\alpha}{8z^2} (1 - 3 \sin^2 \theta) \hat{z} \\ \Omega_{ind} &= a^2 v_0 \frac{3\alpha}{8z^3} \left(1 + \frac{\Gamma}{2}\right) \theta\end{aligned}\tag{2.31}$$

2.3 Simulation

The multipole expansion that is described by Spagnolie& Lauga[7] makes it possible to set up a simulation of an active particle's behavior near a wall, without the need for a full fluid simulation. Such a simulation is described in this section.

2.3.1 General properties

The numerical simulation used for this thesis was constructed in Python (ver 3.8.3). It makes use of the **numpy** package, the **pyplot** and **Axes3D** modules from the **matplotlib** package, and the **optimize** and **Rotation** modules from the **scipy** package.

Natural units

To simplify the notation, the quantities in the simulation are expressed in natural units. Following Spagnolie&Lauga[7], lengths are expressed in units of a , velocities in units of v_0 and forces in units of $\mu a v_0$. Other relevant units follow from this choice of natural units: for instance, time is expressed in units of $a v_0^{-1}$.

2.3.2 Simulating the trajectory of an active particle

The Langevin equations for an active particle in an infinite fluid in 2.11 are written in terms of a continuous time t . Since the simulation must work with discrete time steps, the equations must be rewritten as

$$\begin{aligned}\vec{x}_{0,i+1} &= \vec{x}_{0,i} + \vec{p}(\theta_i, \phi_i) \Delta t \\ \theta_{i+1} &= \theta_i + \xi_{\theta,i}(\theta_i) \\ \phi_{i+1} &= \phi_i + \xi_{\phi,i}(\theta_i)\end{aligned}\tag{2.32}$$

It should be remarked that the noise terms ξ in these equations are not the same as in Equation 2.11. Because these discrete equations describe position rather than velocity, the noise terms are time integrals of those in Equation 2.11. This means that the values $\xi_{k,i}$ are pulled from a Gaussian distribution with variance $2D_k\Delta t$, with $k = \theta, \phi$.

Value of rotational diffusion coefficient

In body frame coordinates, an axisymmetrical particle experiences isotropic rotational diffusion with a diffusion coefficient $D_r = D_{\theta'} = D_{\phi'}$. For a sphere, the rotational diffusion coefficient is given by the Stokes-Einstein relation:

$$D_r = \frac{k_B T}{8\pi\mu a^3} \quad (2.33)$$

where $k_B T$ is the thermal energy and μ is the viscosity of the surrounding fluid. Converted to natural units, this becomes

$$D_r = \frac{k_B T}{8\pi\mu a^2 v_0} \quad (2.34)$$

Thus, the relative strength of rotational diffusion becomes smaller with increasing particle size or velocity.

When the eccentricity is not equal to 1, the rotational diffusion coefficient is expected to deviate from the prediction of a sphere. For this simulation, the value for a sphere was used.

A note on rotational diffusion in different inertial frames

The noise terms ξ_θ and ξ_ϕ depend on θ_i because the simulation works with lab frame coordinates.

A 3D particle can carry out three Euler rotations. These three Euler rotations fully define the orientation of the particle. If one chooses to use lab frame coordinates, the three rotations are around the fixed axes x, y, z . On the other hand, if one uses body coordinates, the inertial frame rotates along with the particle. For the first rotation, the body and lab frames coincide.

Let the initial orientation of the particle ($\theta = 0, \phi = 0$) be along the x axis. With the coordinates as defined in Figure 2.1, one must first rotate the particle by θ around the y axis, then by ϕ around the z axis to obtain the desired orientation.

Rotational diffusion, on the other hand, is understood in body frame coordinates θ', ϕ' . While the first rotation angle θ' coincides with θ in the lab

frame, the second rotation by ϕ' is around the axis z' in the rotated inertial frame. Thus, the rotational diffusion needs to be transformed from one coordinate system to another, as dictated by the equations:

$$\begin{aligned}\xi_{\theta,i}(\theta_i) &= \xi_{\theta',i} + \Delta\theta(\theta_i, \xi_{\phi',i}) \\ \xi_{\phi,i}(\theta_i) &= \Delta\phi(\theta_i, \xi_{\phi',i})\end{aligned}\quad (2.35)$$

where $\xi_{\theta',i}, \xi_{\phi',i}$ are pulled from a Gaussian distribution with variance $2D_r t$. $\Delta\theta$ and $\Delta\phi$ are fully determined by the set of equations:

$$\begin{aligned}\tan \Delta\phi &= \frac{1}{\cos \theta_i} \tan \xi_{\phi',i} \\ \sin \Delta\phi &= \frac{1}{\cos(\theta_i + \Delta\theta)} \sin \xi_{\phi',i} \\ \sin(\theta_i + \Delta\theta) &= \sin \theta_i \cos \xi_{\phi',i}\end{aligned}\quad (2.36)$$

When $\xi_{\phi',i}$ is small, $\Delta\phi$ and $\Delta\theta$ can be expressed directly as:

$$\begin{aligned}\Delta\phi &\approx \arctan \frac{\xi_{\phi',i}}{\cos \theta_i} \\ \Delta\theta &\approx \cot \theta_i - \sqrt{\cot^2 \theta_i + \xi_{\phi',i}^2}\end{aligned}\quad (2.37)$$

The exact transformation is done efficiently using the **Rotation** module from the **scipy** package.

2.3.3 Boundary correction

Steric wall-particle interaction

The particle must be prevented from going through the wall. At low Reynolds numbers, inertia is negligible. Thus, the steric interaction between the particle and the wall will simply make the particle halt when it touches the wall. This was implemented by setting z_0 to the minimum height z_{min} whenever it falls below that point.

For a spherical particle, z_{min} is simply the radius. For an ellipsoidal particle z_{min} is dependent on θ :

$$z_{min} = \sqrt{(a \sin \theta)^2 + (b \cos \theta)^2}\quad (2.38)$$

where a is the semimajor axis and b is the semiminor axis.

Force dipole contribution

Using the expressions in Equation 2.30, the incorporation of the dipole term into the simulation is rather straightforward:

$$\begin{aligned}
 \vec{x}_{0,i+1} &= \vec{x}_{0,i} + \vec{p}(\theta_i, \phi_i) + \frac{3\alpha}{8z_i^2} (1 - 3\sin^2 \theta_i) \hat{z} \Delta t \\
 \theta_{i+1} &= \theta_i + \frac{3\alpha}{8z_i^3} \left(1 + \frac{\Gamma}{2}\right) \theta_i \Delta t + \xi_{\theta,i}(\theta_i) \\
 \phi_{i+1} &= \phi_i + \xi_{\phi,i}(\theta_i)
 \end{aligned} \tag{2.39}$$

Chapter 3

Results

The Langevin equations in Equation 2.39 were solved numerically for a range of values of α . The active velocity was set to $v_0 = 1 \mu\text{ms}^{-1}$ and the semimajor axis to $a = 1 \mu\text{m}$, these being typical values for the particle size and velocity. The temperature was set to room temperature ($T = 300 \text{ K}$), and the viscosity to that of water ($\mu = 1 \times 10^{-3} \text{ Pa s}$). All simulations used time steps $\Delta t = 0.1a/v_0 = 0.1 \text{ s}$. Although the numerical computation used natural units, the results shown here were converted back to SI units, so that they can more easily be compared to experimental results.

3.1 Qualitative observations of particle trajectory

For $\alpha = 0$, the particle trajectories show the expected diffusive behavior. At short timescales the particle moves ballistically, while at long timescales rotational diffusion makes it diffuse isotropically. When α is high enough, the particle aligns parallel to the boundary and diffuses in 2D.

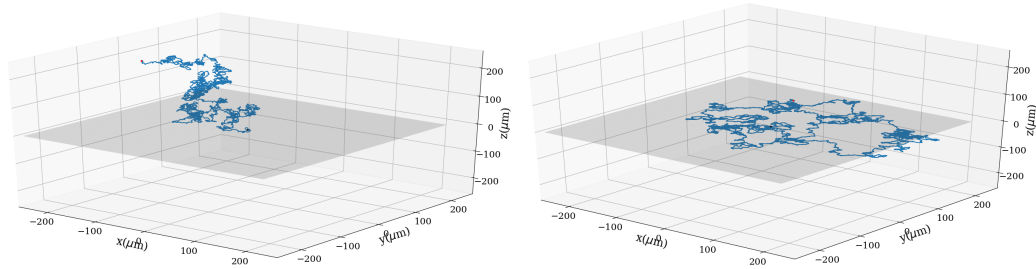


Figure 3.1: Examples of particle trajectories for $\alpha = 0$ (left) and $\alpha = 18$ (right), iterated over $n = 100000$ steps or 10000 seconds.

3.2 Quantification by mean-squared displacement and velocity-velocity correlation

The particle trajectories were quantified by the determination of the mean-squared displacement $\langle |\vec{x}_0|^2(t) \rangle$ and the velocity-velocity correlation $\langle \vec{p}(0) \cdot \vec{p}(t) \rangle$. For both of these functions, the statistical average was taken by dividing the trajectory into blocks and taking the average over all blocks. The resulting plots for different values of α are shown in Figure 3.2. The total number of iterations for these computations was $n = 1000000$. For the mean-squared displacement a block size $\Delta n = 1000$ was used, while for the velocity-velocity correlation the block size was $\Delta n = 100$.

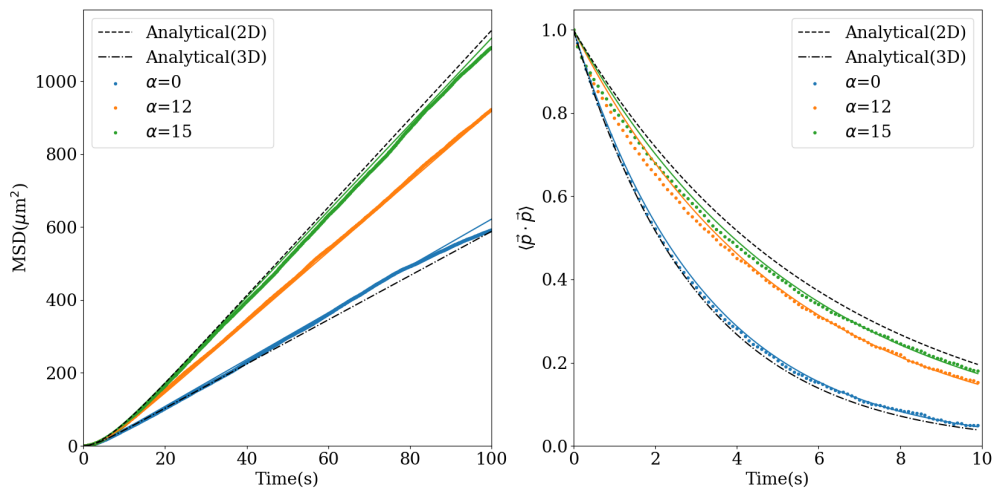


Figure 3.2: Examples of MSD and velocity correlation plots from which the diffusion coefficient and rotation time are determined, respectively.

3.3 Determination of diffusion coefficient and rotation time

From the mean-squared displacement and velocity-velocity correlation functions, the effective diffusion coefficient and rotation time were determined. The rotation time τ_r is related to the velocity-velocity correlation through the exponential relationship

$$\langle \vec{p} \cdot \vec{p} \rangle = e^{-t/\tau_r} \quad (3.1)$$

while the translational diffusion coefficient D was determined from the mean-squared displacement at long timescales:

$$\langle |\vec{x}_0|^2 \rangle = 6Dt \quad (3.2)$$

Both for the mean-squared displacement and the velocity-velocity correlation, the trajectory was cut up into blocks for which $|\vec{x}_0|^2(t)$ and $\vec{p}(0) \cdot \vec{p}(t)$ were determined individually. The average was then taken over all blocks. The mean-squared displacement was fitted with the relation:

$$\langle |\vec{x}_0|^2 \rangle - \langle |\vec{x}_0|^2 \rangle|_{t_0} = 6D(t - t_0) \quad (3.3)$$

where $t_0 = 10\tau_r$, as the mean-squared displacement is in the linear regime at this lagtime.

For the fitting of the velocity-velocity correlation, a semilog scale was used:

$$\ln \langle \vec{p} \cdot \vec{p} \rangle = -\frac{t}{\tau_r} \quad (3.4)$$

In the chosen range of α , a transition is observed between 2D and 3D diffusive behavior for the rotation time and diffusion coefficient (Figure 3.3). This is as expected, since the induced angular velocity tends to make the particle align parallel to the wall (see Eq. 2.30).

In the long-time limits of Equations 2.15 and 2.18, the translational diffusion coefficient is related to the rotation time by the linear relation:

$$D = \frac{1}{3}v_0^2\tau_r \quad (3.5)$$

There is no significant deviation from this linear relation in the observed crossover between 3D and 2D diffusion, as demonstrated in Figure 3.4.

The value of α where the transition from 3D to 2D takes place is expected to depend on the velocity v_0 , semimajor axis a and the eccentricity e . A

larger velocity v_0 or semimajor axis a should lower the value of α at which the transition takes place, as this lowers the relative rotational diffusion coefficient (see Eq.2.34). A lower eccentricity also makes the transition shift to a lower value of α , as the induced angular velocity is higher in this case (Eq.2.30). Values for $e = 0.8$ are also included in Figure 3.3 to illustrate this shift.

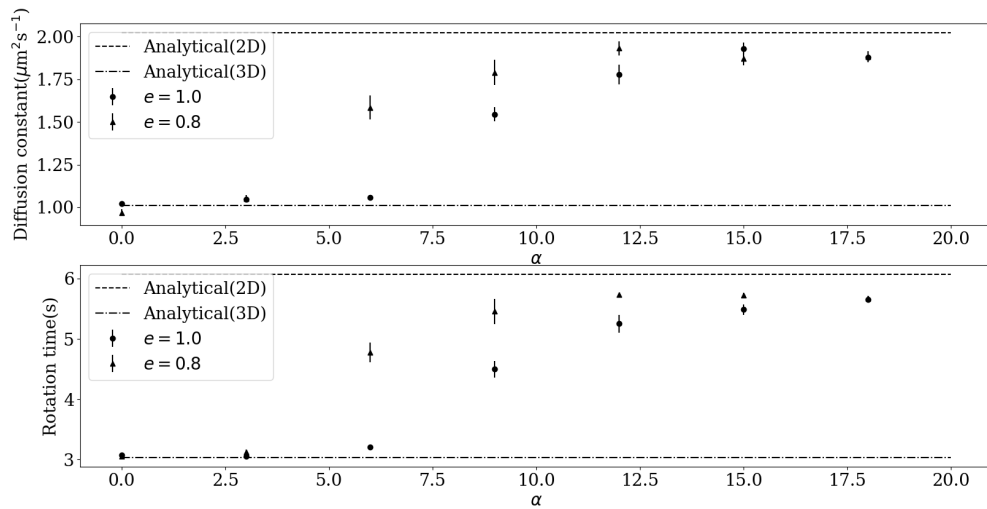


Figure 3.3: Diffusion coefficient and rotation time for the chosen range of values of α , for eccentricities $e = 1$ and 0.8 .

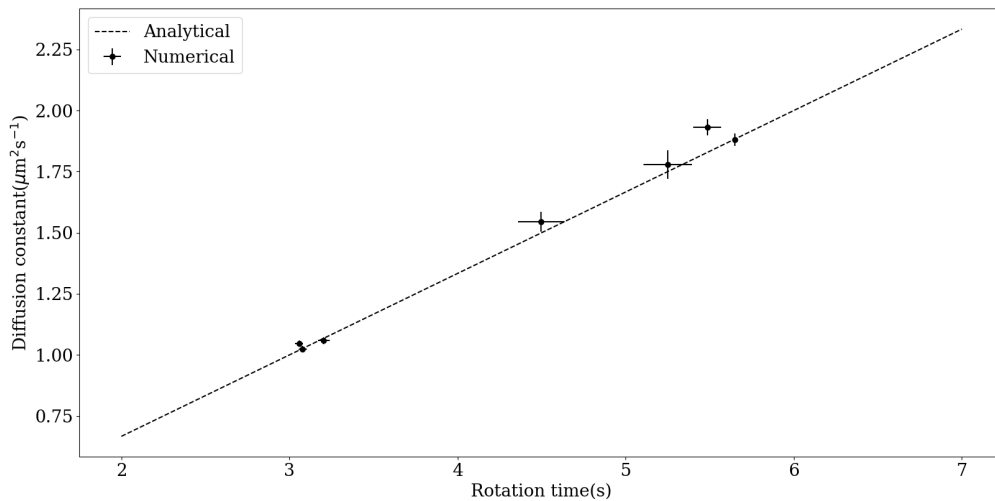


Figure 3.4: Relation between the translational diffusion coefficient and rotation time for the range of α shown in Fig. 3.3.

3.4 Analytical calculation

To complement the results of numerical simulation, we now aim to establish an analytical model for the 3D/2D transition. This is done by finding the Fokker-Planck equation, which describes the time evolution of the probability P of a certain configuration. We use the notation $\vec{R} = (x_0, y_0, z_0, \theta, \phi)$ for the coordinates of the particle. The correlation functions that are used to characterize the system, namely the mean-squared displacement and the velocity-velocity correlation, are then obtained from the integrals:

$$\begin{aligned} \frac{\partial \langle |\vec{x}_0|^2(t) \rangle}{\partial t} &= \int d\vec{R} |\vec{x}_0|^2 \frac{\partial P(\vec{R}, t')}{\partial t} \\ \frac{\partial \langle \vec{p}(0) \cdot \vec{p}(t) \rangle}{\partial t} &= \int d\vec{R} \vec{p}(\theta = 0, \phi = 0) \cdot \vec{p}(\theta, \phi) \frac{\partial P(\vec{R}, t)}{\partial t} \end{aligned} \quad (3.6)$$

These integrals are taken over the whole phase space, with the probability obeying the normalization constraint:

$$\int d\vec{R} P(\vec{R}, t) = 1 \quad (3.7)$$

For our system where we truncate the multipole expansion to the first order, we have obtained the Fokker-Planck equation:

$$\begin{aligned} \frac{\partial P}{\partial t} &= -\frac{\partial}{\partial x}(v_0 \cos \theta \cos \phi P) - \frac{\partial}{\partial y}(v_0 \cos \theta \sin \phi P) - \frac{\partial}{\partial z} \left[v_0 \left(\sin \theta - \frac{3a^2 \alpha}{8z^2} (1 - 3 \sin^2 \theta) \right) P \right] \\ &+ \frac{\partial}{\partial \theta} \left[\frac{3v_0 a^2 \alpha}{8z^3} \left(1 + \frac{\Gamma}{2} \right) \theta P \right] + D_{\theta\theta} \frac{\partial^2 P}{\partial \theta^2} + D_{\phi\phi} \frac{\partial^2 P}{\partial \phi^2}, \end{aligned} \quad (3.8)$$

However, we have not yet been able to fully work out the correlation functions.

Chapter 4

Discussion

The multipole expansion coefficient α can only be determined exactly through a full numerical calculation. However, it is fixed for a given particle geometry and propulsion mechanism, and one can predict how the results change when the semimajor axis a or velocity v_0 are changed. Some reservations do need to be made when comparing the results from Chapter 3 to experimental findings. These are given in this chapter.

4.1 Limitations of simulation

The simulation must work with discrete time steps Δt . This discrete nature of the simulation will impact the results for large forces and velocities. In particular, the hydrodynamic torque that causes the particle to align parallel to the wall will overshoot if the time step Δt is too large. Thus, an effect can be seen where the particle stops aligning to the wall and goes back to 3D diffusion as the involved forces become larger. This is purely an artifact of the simulation, as the particle will once again align parallel to the wall when a sufficiently small time step is used.

4.2 Higher-order terms

The higher-order terms in the multipole expansion can only be neglected if the particle is far enough away from the wall. After the force dipole term, the three second-order terms are the next most relevant to consider. These are the source dipole, the force quadrupole and the rotlet dipole term. The source dipole and force quadrupole contributions both result in a constant rotation in θ , and an attraction to or repulsion from the wall

depending on θ . The rotlet dipole is relevant for chiral particles, and results in circular movement in the x - y plane.

In this thesis α was varied. One can similarly vary the other coefficients β, γ, τ to explore the higher-order terms.

4.3 Application to experiments

There are two obvious types of applications to which the hydrodynamic description considered in this thesis is relevant. First, it is relevant to self-propelled particles that naturally tend to move near a boundary. Examples of these are sperm cells approaching an egg cell, or synthetic swimmers that travel through veins to carry medicine[11]. Second, particles that are observed under a microscope may swim close to a substrate by necessity. We make special note of one type of synthetic self-propelled particle, namely catalytic Pt-coated swimmers, which were the initial motivation for this thesis. For such swimmers, it must be noted that other effects may play a role. In particular, it has been shown that the propulsion mechanism has an electrodynamic component[12].

Chapter 5

Conclusions

The far-field behavior of an axisymmetrical particle near a wall was investigated, using the established multiple expansion theory. The effect of a wall on the force dipole term in the presence of rotational diffusion was explored via numerical simulation. This was quantified by the rotation time τ_r and long-time translational diffusion coefficient D for varying values of the first-order expansion coefficient α . We find that a transition takes place between three-dimensional diffusion and two-dimensional diffusion parallel to the wall. This is reflected in the rotation time and diffusion coefficient. For a spherical particle with active velocity $\vec{v}_0 = 1 \mu\text{ms}^{-1}$ and radius $a = 1 \mu\text{m}$, this transition takes place at $\alpha \approx 9$.

Bibliography

- [1] Howard C. Berg and Douglas A. Brown. Chemotaxis in *Escheria Coli* analyzed by three-dimensional tracking. *Nature*, 239:500–504, 1972.
- [2] D.M. Woolley. Motility of spermatozoa at surfaces. *Reproduction*, 126:259–270, 2003.
- [3] W.F. Paxton, K.C. Kistler, C. C. Olmeda, A. Sen, S.K. St. Angelo, Y. Cao, T.E. Mallouk, P.E. Lammert, and V.H. Crespi. Catalytic nanomotors: Autonomous movement of striped nanorods. *J. Am. Chem. Soc.*, 126:13424–13431, 2004.
- [4] R. Dreyfus, J. Baudry, M.L. Roper, M. Fermigier, H.A. Stone, and J. Bibette. Microscopic artificial swimmers. *Nature*, 437:862–865, 2005.
- [5] J.R. Howse, R.A.L. Jones, A.J. Ryan, T. Gough, R. Vafabakhsh, and R. Golestanian. Self-motile colloidal particles: From directed propulsion to random walk. *Physical Review Letters*, 99, 2007.
- [6] R.P. Doherty, T. Varkevissier, M. Teunisse, J. Hoecht, S. Ketzetzi, S. Ouhajji, and D.J. Kraft. Catalytically propelled 3D printed colloidal microswimmers. *Soft Matter*, 16:10463–10469, 2020.
- [7] Saverio E. Spagnolie and Eric Lauga. Hydrodynamics of self-propulsion near a boundary: predictions and accuracy of far-field approximations. *J. Fluid. Mech.*, 700:105–147, 2012.
- [8] C. Bechinger, R. Di Leonardo, H. Lowen, C. Reichhardt, G. Volpe, and G. Volpe. Active particles in complex and crowded environments. *Rev. Mod. Phys.*, 88, 2016.
- [9] J.R. Blake. A note on the image system for a stokeslet in a no-slip boundary. *Proc. Camb. Phil. Soc.*, 70:303–310, 1971.

- [10] O.A. Ladyzhenskaya. *The mathematical theory of viscous incompressible flow*. Gordon&Breach, 2nd edition, 1969.
- [11] F. Wong, K.K. Day, and A. Sen. Synthetic micro/nanomotors and pumps: Fabrication and applications. *Annu. Rev. Mat. Res.*, 46:407–432, 2016.
- [12] A. Brown and W. Poon. Ionic effects in self-propelled Pt-coated janus swimmers. *Soft Matter*, 10:4016–4027, 2014.